Supplementary Information

A flexible piezoelectric sensor based on a piezoelectric composite film with high sensitivity and excellent thermal stability for multi-scenario applications

Chungang Li, Changhong Yang*, Yaoting Zhao, Gensheng Dong, Xiujuan Lin, Shifeng Huang

Shandong Provincial Key Laboratory of Preparation and Measurement of Building Materials, University of Jinan, 250022 Jinan, China

*Corresponding author, E-mail address: mse_yangch@ujn.edu.cn

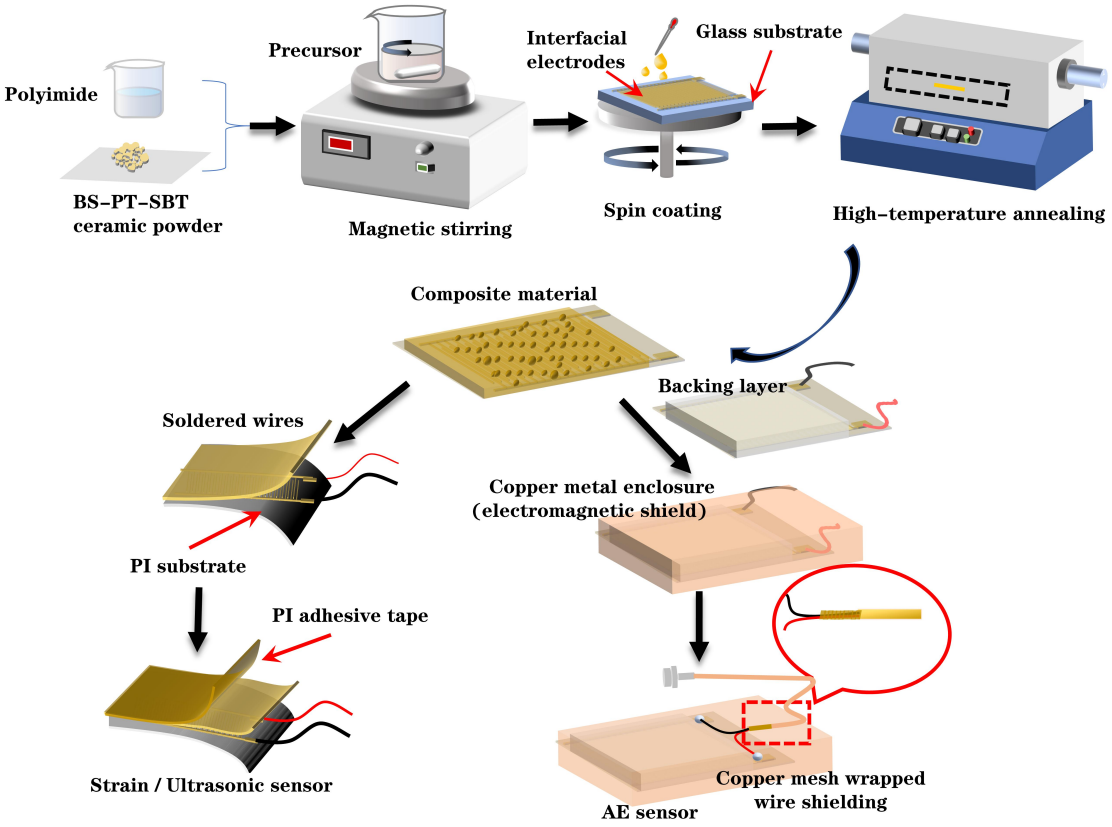

Fig. S1. Fabrication process of piezoelectric sensors.

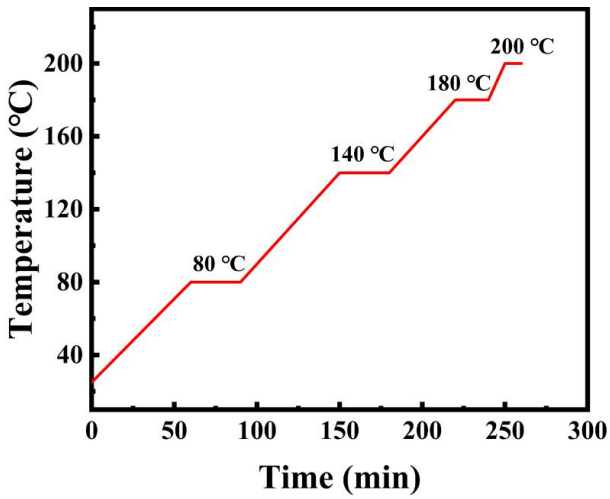

Fig. S2. Solidification process for the BS-PT-SBT-PI film.

Table S1 The structural parameters of the interdigital electrode.

ID electrodes Model	Number of fingers	Finger width (μm)	Finger distance (μm)
Type I	34	100	200
Type II	50	100	100
Type III	100	50	50

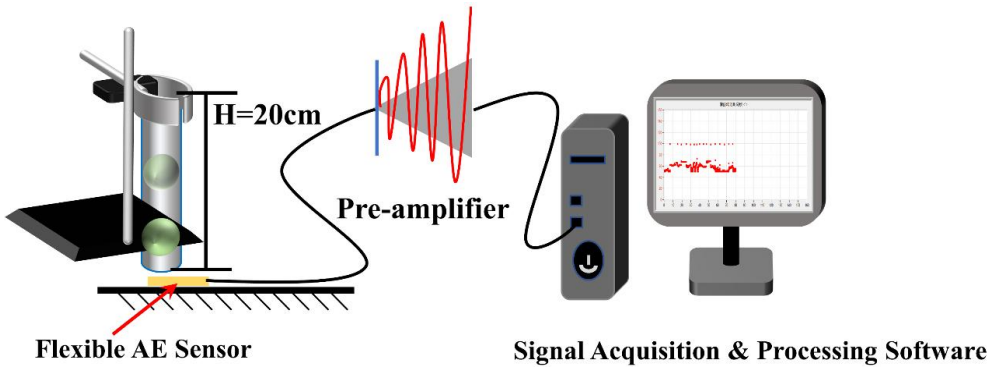

Fig. S3. Schematic diagram of a falling ball method.

In this paper, the prepared sensors are tested by a falling ball method. The falling ball test system consists of a self-made AE sensor, the Al plate, a pre-signal amplifier, and a PCI-2 AE acquisition instrument. The AE sensor is attached to the Al plate to be tested through a coupling agent. A small zirconium sphere is used as AE source by free-falling from a height of 20 cm.

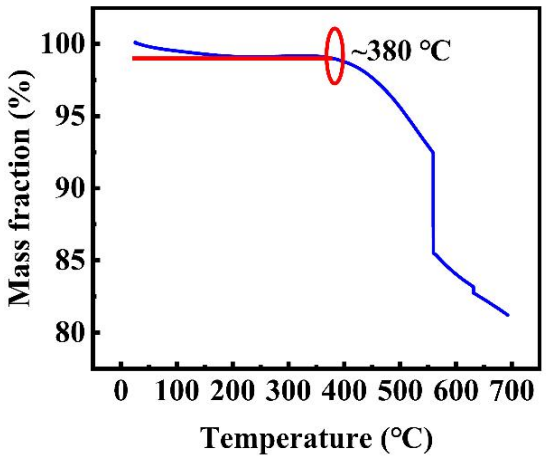

Fig. S4. TGA plot of composite film with 50 wt% BS-PT-SBT.

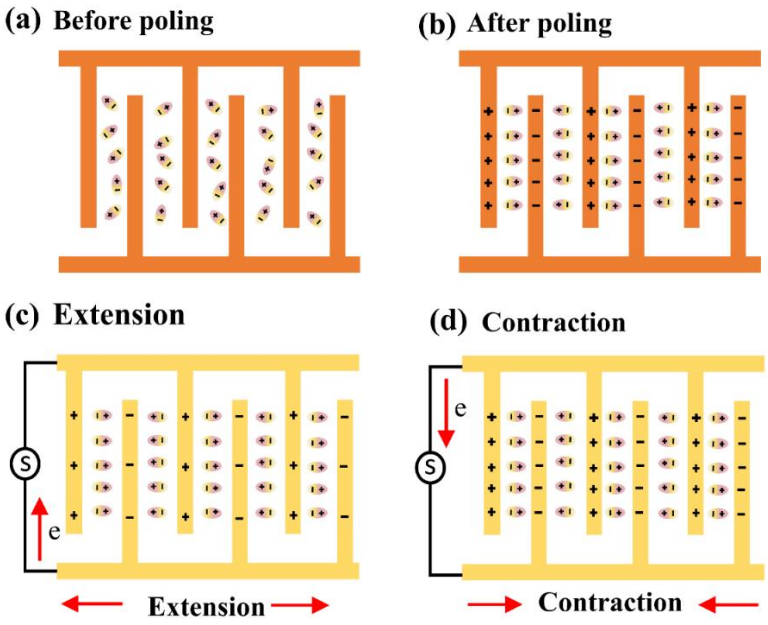

Fig. S5. Schematic illustration of dipole alignment during the poling and applied pressure processes. (a) Dipoles align randomly at the original state. (b) After poling, the dipoles align in the direction along the electric field. (c) The piezoelectric potential is formed as a compressive force is applied on the piezoelectric composite film. (d) Electrons flow back along the opposite direction when the compressive force is released.

As shown in Fig. S5 (a), prior to the polarization process, the ferroelectric domains are randomly arranged in the BS-PT-SBT within the PI matrix. However, when a strong electric field is applied to the composite film, the ferroelectric domains tend to align with the direction of the electric field, as exhibited in Fig. S5 (b). The rearranged domains maintain a permanent polarization even after the poling voltage is removed, resulting in a high piezoelectric potential in response to external force. In the poled composite film without applied external force, there is no electrical signal output due to the electrical balance. For example, taking a compressive force applied to the film, the distance between the two-finger electrodes will increase, which may contribute to an increase of the internal polarization of the composite film. Therefore, to maintain the balance of the piezoelectric potential, the free electrons will flow from high potential to low potential and accumulate on the electrode surfaces through an external circuit, as shown in Fig. S5 (c). As a result, an electric pulse will be generated in responding to the mechanical stress. Furthermore, when the external pressure on

the device is removed, the distance between two neighbor electrodes will recover to the original state, and thus the piezoelectric potential will disappear, as shown in Fig. S5 (d). The free electrons accumulate at the electrode flow back, which can generate a negative electrical signal. Consequently, alternative pulse voltages/currents are generated in the circuit connecting to the piezoelectric composite film. Similarly, the converse phenomenon can be happened when the film is subjected to a tensile force originating from mechanical bending.

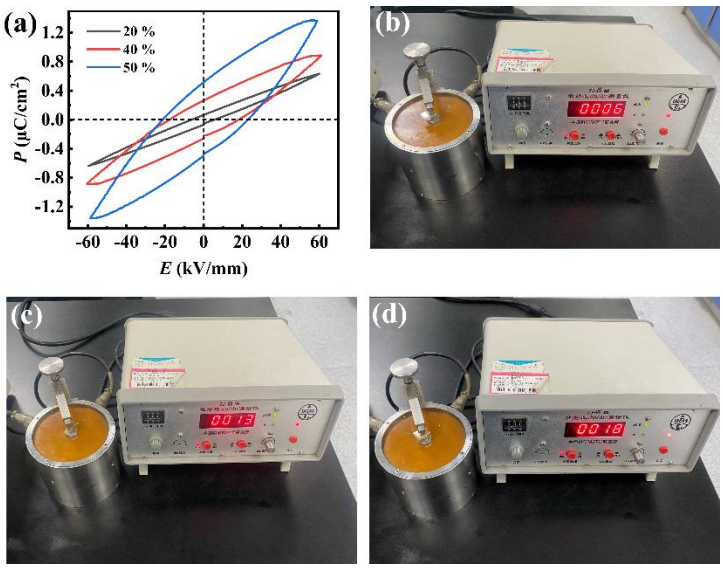

Fig. S6. (a) *P-E* loops of the composite films at the same electric field. Piezoelectric coefficient d_{33} values of composite films with different mass fractions: (b) 20%, (c) 40%, and (d) 50%.

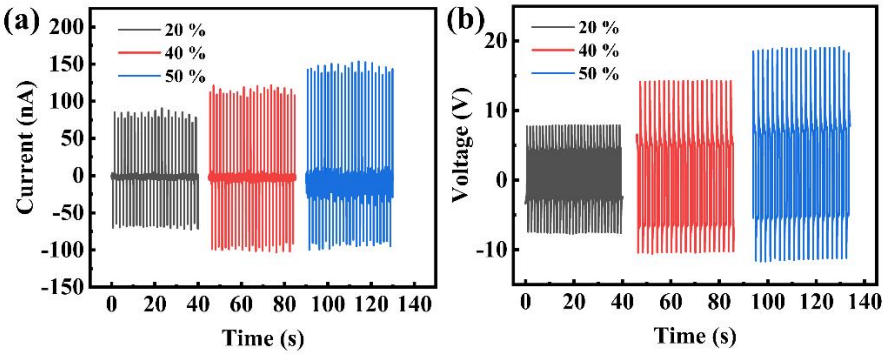

Fig. S7. (a) Output currents and (b) output voltages of the composite films with 20, 40, and 50 wt% BS-PT-SBT under the same condition of cyclic strikes.

Fig. S8. The BS-PT-SBT-PI film with 60% weight fraction ceramics.

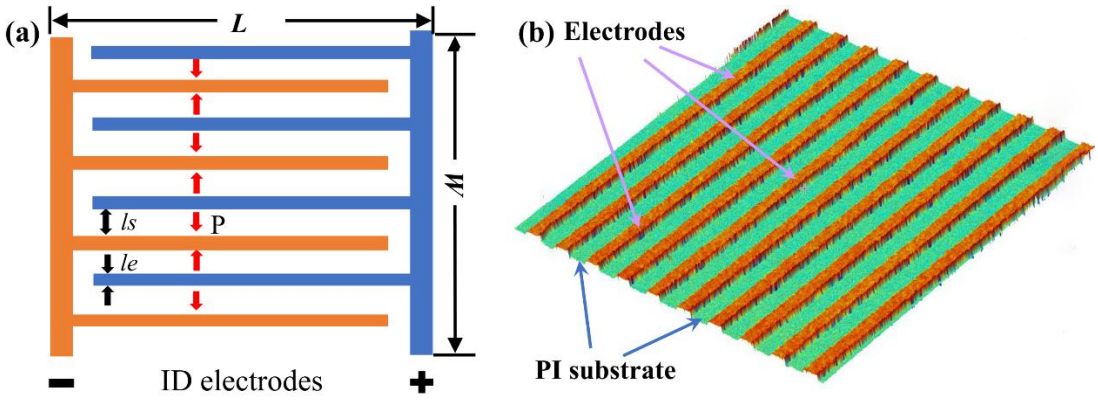

Fig. S9. (a) Structural diagram of the ID electrodes. (b) 3D image of Type III ID electrodes.

Fig. S9(a) shows the structural diagram of ID electrodes. Each ID electrode has the fixed the length (L) of 2.5 cm and width (W) of 2 cm. The different distance sizes between adjacent fingers (ls) and the width of a single finger (le) correspond to Type I, Type II ID, and Type III ID electrodes, as revealed in the Table S1. Fig S9 (b) displays the 3D image of the flexible Type III ID electrode obtained by laser confocal microscopy. The height of each finger on this electrode is consistent, and the distance between the fingers is basically the same.

Table S2 The calculated forces based on different weights, and corresponding output voltages.

m (kg)	g (N/kg)	h (m)	Δt (s)	$F = \Delta mgh/\Delta t$ (N)	Voltage (V)
0.002	9.8	0.3	0.02	0.29	0.90
0.005	9.8	0.3	0.02	0.74	1.36
0.02	9.8	0.3	0.02	2.94	15.17
0.03	9.8	0.3	0.02	4.41	27.61

Note: the voltage values are obtained by calculating the average of output voltages.

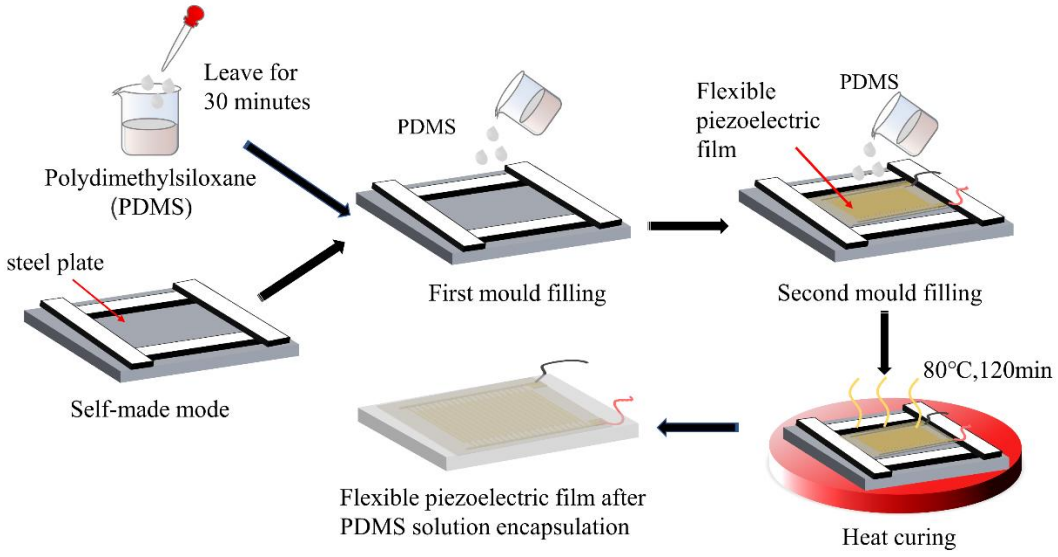

Fig. S10. The diagram of flexible device encapsulation process.

Polydimethylsiloxane (PDMS, Sylgard 184) prepolymer and curing agent were mixed at a weight ratio of 10:1 using a planetary centrifugal mixer for 5 min at 400 rpm.

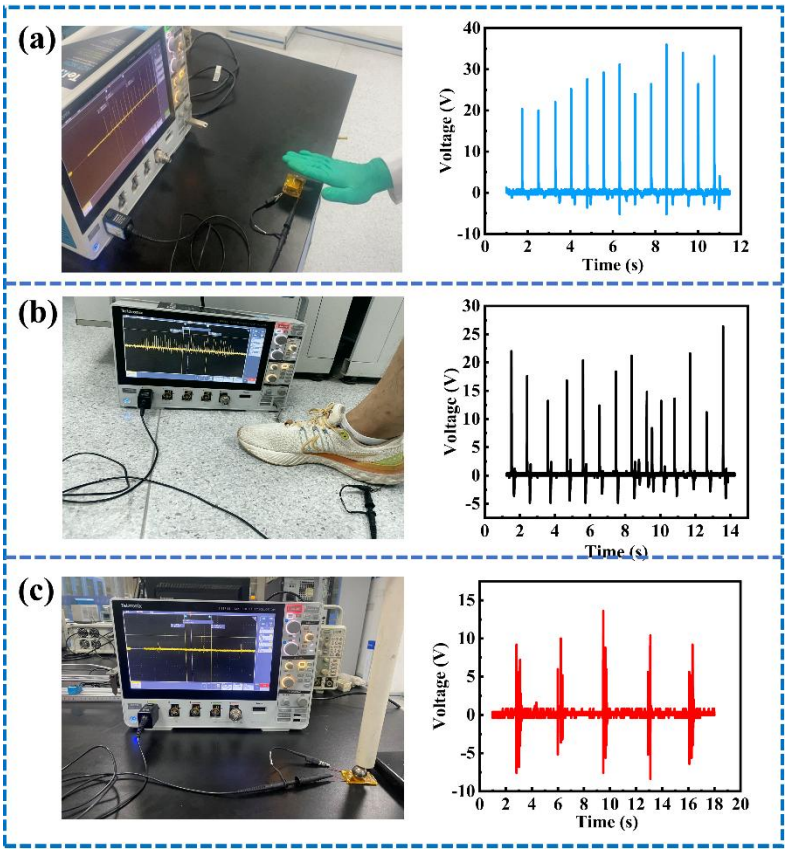

Fig. S11. The output voltages of flexible film under the different impact modes: (a) hand, (b) foot, and (c) steel ball.

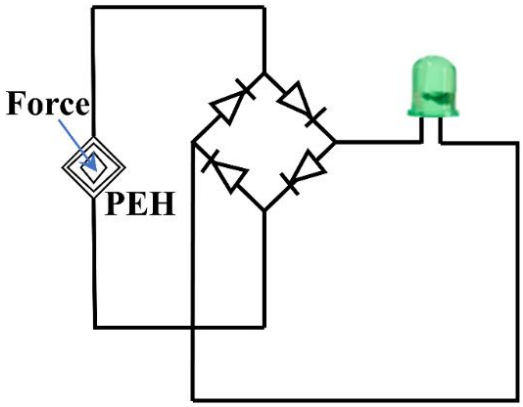

Fig. S12. Schematic diagram of rectifier circuit.

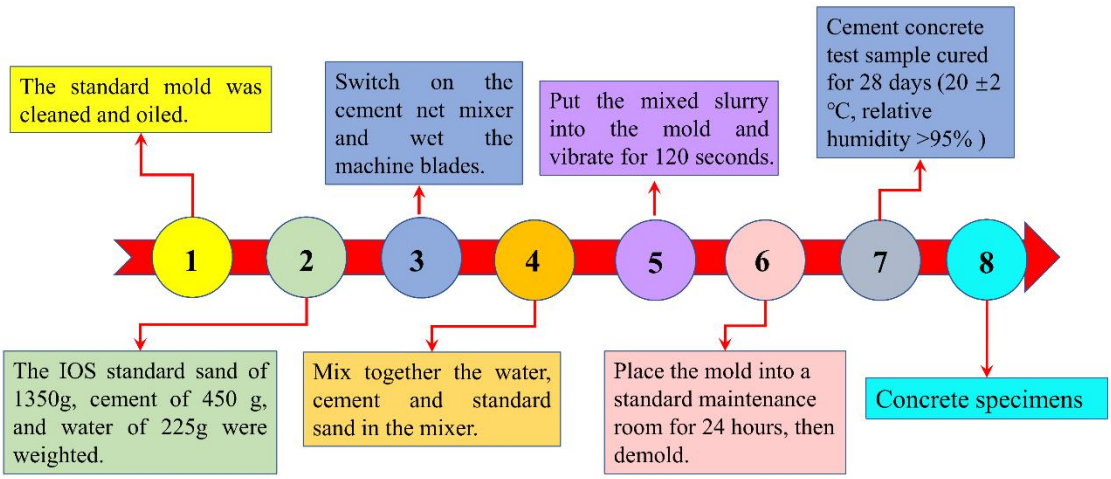

Fig. S13. Procedure for the preparation of concrete specimens according to the specification GB/T 17671-2021 of China.

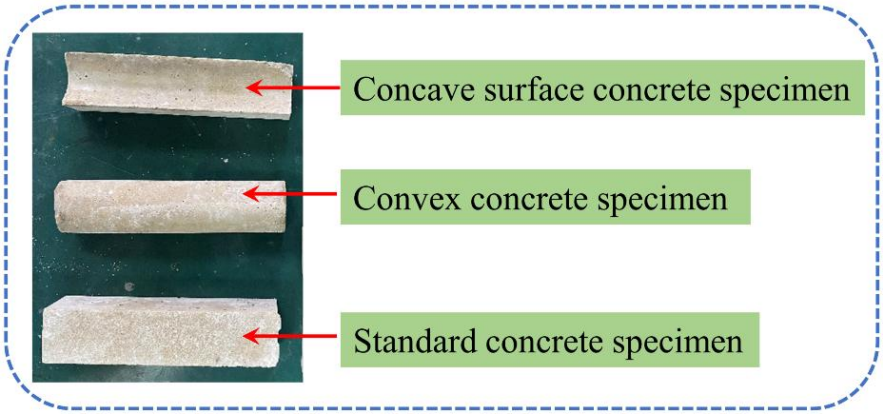

Fig. S14. Concrete specimens with different curved structures.

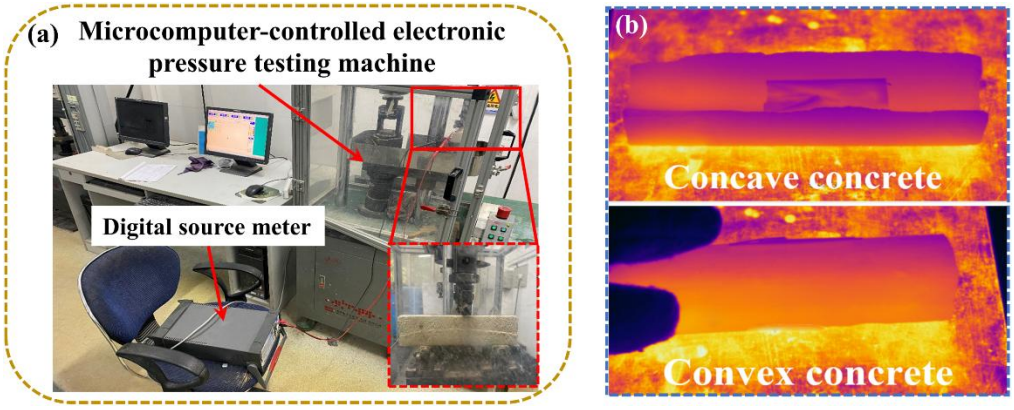

Fig. S15. (a) The photograph for the three-point loading test system. (b)The infrared thermographic images of the concave and convex concrete specimens with sensor heated at 200 °C.

In this system, a microcomputer-controlled electronic pressure testing machine is treated as the loading equipment, and a digital source meter is used to receive the output voltage signals.

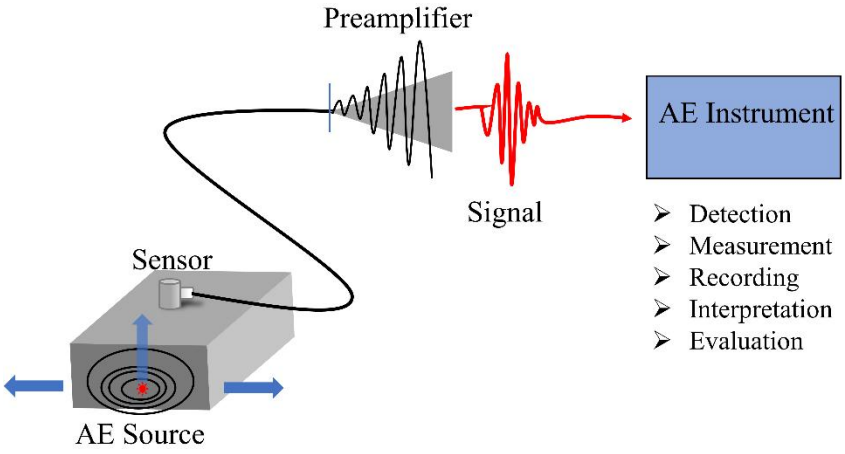

Fig. S16. The schematic diagram of the AE monitoring system.

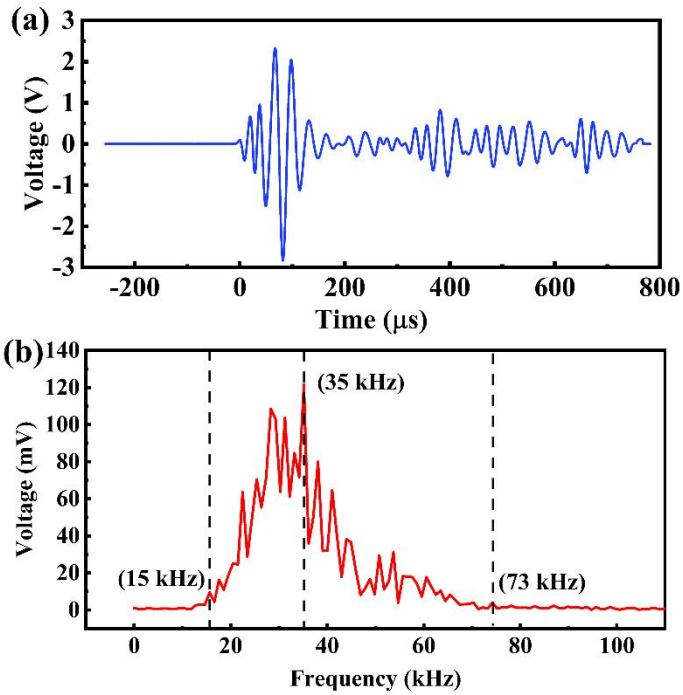

Fig. S17. Wave and frequency testing of AE sensor: (a) waveform diagram and (b) frequency domain plot.

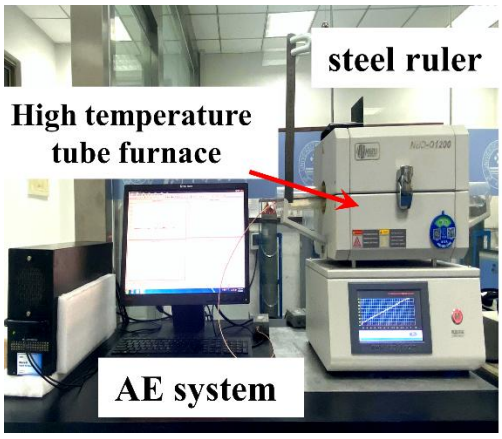

Fig. S18. An in-situ high-temperature test system of falling ball method.

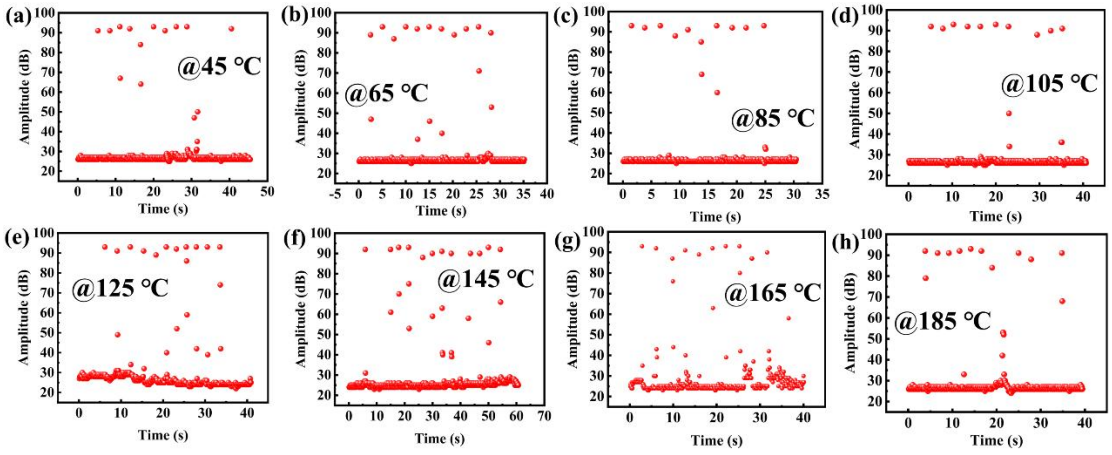

Fig. S19. Amplitude signals at different temperatures: (a) 45 °C, (b) 65 °C, (c) 85 °C, (d) 105 °C, (e) 125 °C, (f) 145 °C, (g) 165 °C, and (h) 185 °C.

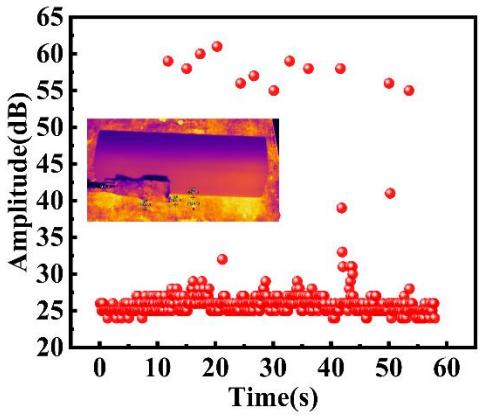

Fig. S20. Time-domain diagram for the sensor on the standard concrete structure. The inset is the infrared thermogram of the standard concrete specimen.

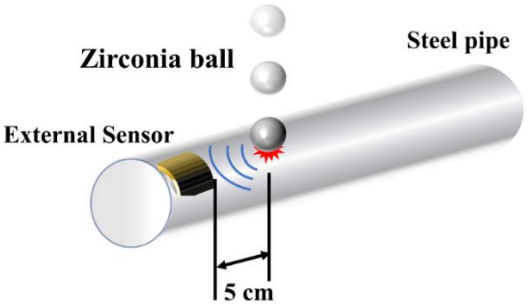

Fig. S21. The schematic diagram of the falling ball method test for the sensor attached outside steel pipe.

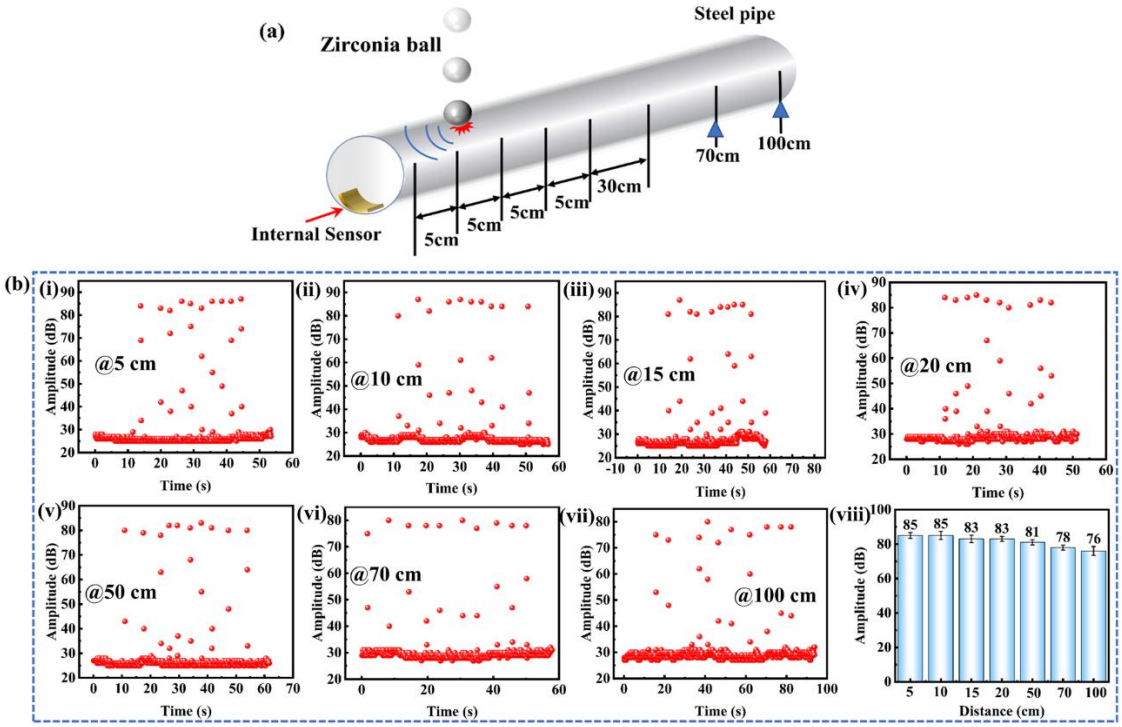

Fig. S22. (a) The schematic diagram of the falling ball method test for the sensor attached inside a steel pipe. (b) Amplitudes of different sound source locations of 5-100 cm.

As shown in Fig. S22(b), the AE sensor collects the amplitude signals at the sound sources from 5~100 cm, respectively, where the average amplitude signal is reduced from 85 dB to 76 dB, with a drop rate of only about 10 %.

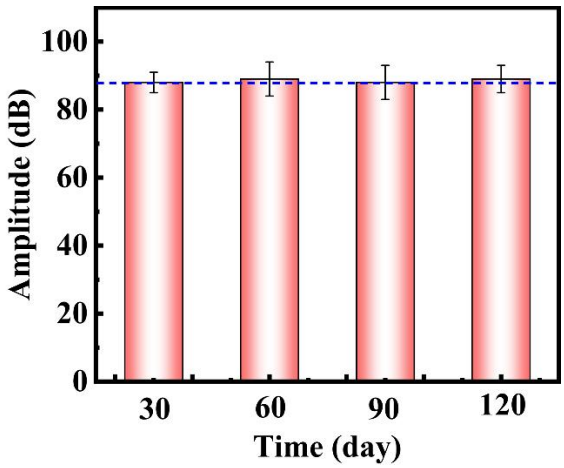

Fig. S23. Amplitude *versus* time for the AE sensor.